Journal of Molecular Structure 1222 (2020) 128854

Contents lists available at ScienceDirect

Journal of Molecular Structure

journal homepage: http://www.elsevier.com/locate/molstruc

Articaine interaction with phospholipid bilayers

Érica Teixeira Prates [a, 1], Gustavo Henrique Rodrigues da Silva [b], Thais F. Souza [b], Munir S. Skaf [a], Mónica Pickholz [c, **], Eneida de Paula [b, *]

[a] Institute of Chemistry, Center for Computational Engineering and Sciences, University of Campinas, UNICAMP, Campinas, São Paulo, Brazil
[b] Department of Biochemistry and Tissue Biology, Institute of Biology, University of Campinas, UNICAMP, Campinas, São Paulo, Brazil
[c] Department of Physics, Faculty of Exact and Natural Sciences, University of Buenos Aires & IFIBA, CONICET, Buenos Aires, Argentina

ARTICLE INFO

Article history:
Received 6 May 2020
Received in revised form
24 June 2020
Accepted 7 July 2020
Available online 11 July 2020

Keywords:
Local anesthetics
Articaine
Fluorescence
NMR
Molecular dynamics

ABSTRACT

Local anesthetics promote analgesia by interacting with excitable membranes. Articaine (ATC) has a unique composition among local anesthetics as it possesses a thiophene instead of the typical phenyl ring. Aiming to characterize the interaction of neutral articaine (nATC) with phospholipid membranes, we have employed a synergistic approach of experimental and computational techniques. Fluorescence measurements supported nATC partitioning into the membranes, since its intrinsic fluorescence anisotropy increased from 0.03 in water to 0.29 in the presence of egg phosphatidylcholine (EPC) liposomes, and the fluorescence of AHBA, a probe that monitors the water-membrane interface, was quenched by nATC. ^{1}H NMR experiments revealed changes in the chemical shifts of articaine and EPC hydrogens after partitioning, and shorter T_1 values of nATC hydrogens when inserted into the EPC vesicles. Contacts of nATC and the phospholipid polar head group were inferred from 2D-NOE. Taken together, these results indicate a superficial insertion of the nATC molecules inside EPC bilayers. This conclusion was confirmed by molecular dynamics simulations, which allowed the identification of the key interactions underlying the preferential location of nATC in the bilayer. Contrary to what is often stated (that articaine is a high lipophilic local anesthetic agent) our results place ATC among the hydrophilic ones, such as lidocaine, prilocaine, and mepivacaine, for which the water/membrane interface is the preferred location.

1. Introduction

Local anesthetics (LA) are pain relief drugs used in dentistry and medicine. Despite being extremely used, the search for more effective and safe anesthetic agents is still an object of interest for the scientific community, because it would provide significant improvement in patient care [1–4]. Most LA are relatively hydrophobic ionizable amines that undergo partitioning into lipid membranes. Their mechanism of action involves reversible interaction with the voltage-gated sodium channels of neuronal membranes [5,6] modulated by partitioning into the lipid phase [7]. The partition of the neutral (n) species is favored over the protonated (p) one, and the neutral form is also associated with higher anesthetic potency [3,7].

Articaine (ATC) was introduced in 1976 as the unique amide local anesthetic with an ester group and a thiophene ring [8,9]. It became widely used in dentistry, and Malamed et al. proposed that its thiophene group led to increased liposolubility and the ability to penetrate the nerve sheath [10]. However, the partition coefficient of uncharged ATC species (nATC) between octanol and water ($P_{oct} = 257$ [11]) is relatively low and similar to those of procaine, mepivacaine, prilocaine, and lidocaine [5], which are classified as hydrophilic LA agents [12,13]. Moreover, the onset of action of articaine is fast (2–3 min for blockade in dentistry) and comparable to those of mepivacaine, prilocaine, and lidocaine [14]. Finally, the clinical doses for infiltrative anesthesia with articaine (4%) is closer to those of prilocaine (3%), mepivacaine (2–3%), and lidocaine

* Corresponding author. Departamento de Bioquímica e Biologia Tecidual, Instituto de Biologia, UNICAMP, Rua Monteiro Lobato, 255, CEP 13083862, Campinas, São Paulo, Brazil.
** Corresponding author. Departamento de Física, Facultad de Ciencias Exactas y Naturales, Universidad de Buenos Aires & IFIBA, CONICET, Buenos Aires, 1428, Argentina.
E-mail addresses: ericatprates@gmail.com (É.T. Prates), gustavohrs@gmail.com (G.H. Rodrigues da Silva), tha.franco.s@gmail.com (T.F. Souza), skaf@unicamp.br (M.S. Skaf), mpickholz@df.uba.ar (M. Pickholz), depaula@unicamp.br (E. de Paula).
[1] Present address: Biosciences Division, Oak Ridge National Laboratory, Oak Ridge, TN 37830, USA.

https://doi.org/10.1016/j.molstruc.2020.128854
0022-2860/

(2–3%), than to the doses used with more hydrophobic anesthetics (0.5%), such as bupivacaine, tetracaine, and etidocaine [15].

Song et al. [16] have used ^{13}C and ^{31}P nuclear magnetic resonance (NMR) to analyze the interaction of articaine with distearoylphosphatidylcholine membranes and showed that there is a decrease in the membrane packing in the region of the lipid polar head groups in the presence of ATC at pH 10.0. Later, the authors have shown that ATC decreases the phase transition temperature of both palmitoyl-oleyl and stearoyl-oleyl phosphatidylserine (PS) liposomes, as well as it increases the area per lipid in prokaryote membranes, suggesting intercalation of articaine between the lipids, at physiological pH [17]. Molecular dynamics (MD) simulations revealed that nATC is inserted deeper in dimyristoylphosphatidylcholine membranes than the protonated articaine (pATC) species [11,18]. Moreover, MD simulations suggested the formation of intramolecular hydrogen bonds between the carbonyl oxygen of the methoxycarbonyl group and the secondary amine of nATC in palmitoyloleyl phosphatidylcholine (POPC) bilayers. No equivalent internal bond is observed in other LA agents [19]. Despite these findings, there are no experimental or computational studies positing the higher lipophilicity character of articaine molecule relative to other clinically used LA.

In this work, we have examined the interactions of nATC with lipid membranes using experimental (fluorescence, NMR) and computational (MD) approaches. The experiments were conducted at a pH (9.0–9.4) high enough to assure that articaine (pKa = 7.8 [20]) was fully in the neutral form, but not as high as to promote the alkaline hydrolysis of the anesthetic. Complementary analyses were performed with MD simulations both for nATC and pATC in POPC lipid bilayers.

2. Materials and Methods

2.1. Materials

Egg phosphatidylcholine (EPC), deuterated water (D_2O, 99.9%), and Chelex resin were obtained from Sigma-Aldrich (St. Louis, MO, USA). Articaine hydrochloride was donated by Aventis Pharma (Suzano, SP, Brazil). All the other reagents used in this study were of analytical grade.

2.2. Membrane preparation

Liposomes were obtained by evaporating stock chloroform solutions of EPC under a stream of nitrogen. The samples were left under vacuum for no less than 2 h to remove residual solvent. The lipid was then suspended in the appropriate aqueous solution (0.025 M borate buffer, pH 9.0 for fluorescence, or D_2O for NMR experiments) and large multilamellar vesicles were obtained after 3 min of vortexing, at ambient temperature (25 °C).

For the fluorescence experiments large unilamellar vesicles (LUV) were prepared by repeated – 15 cycles – extrusion of the multilamellar vesicles within 0.1 μm polycarbonate membrane filters, in an extruder (Lipex Biomembranes Inc., Vancouver, VA, Canada). To avoid light scattering effects in the fluorescence measurements, LUV concentration was set to 0.5 mM.

The small unilamellar vesicles (SUV) analyzed by NMR were obtained by sonication of the large multilamellar vesicles. The samples were sonicated until a clear solution was yielded (*ca*. 15 min), using a Sonics and Materials equipment (Newtown, CT. USA). During sonication the temperature was kept at 0–4 °C by intermittent (1 min) agitation cycles in ice-water bath. The sonicated samples were centrifuged with Chelex resin at 1000×*g* for 20 min to remove residual large particles and any titanium from the sonicator tip. The concentrations of EPC and ATC used in the NMR experiments were 100 mM and 130 mM, respectively; the pH of samples (with or without ATC) was adjusted with NaOD or DCl solutions to 9.4.

2.3. Fluorescence experiments

The static fluorescence experiments were conducted in a F4500 Hitachi equipment. The N-hexadecyl-benzamide, AHBA, probe [21] was incorporated into the LUV up to 0.2 mol % of the EPC concentration (0.5 mM). Fluorescence emission was measured between 350 and 500 nm following excitation at 345 nm, in the presence of increasing amounts of ATC (0–15 mM). The intrinsic fluorescence of articaine was also measured, in solution (0.025 borate buffer, pH 9.0) or in the presence of 1 mM LUV. After irradiation at 273 nm, the anisotropy of the emitted ATC fluorescence at 353 nm was calculated [22].

2.4. Nuclear magnetic resonance (NMR) experiments

^1H NMR spectra were collected with a Varian Inova 500AS spectrometer operating at 499.69 MHz for ^1H (at the Brazilian National Synchrotron Laboratory, LNLS, Campinas, SP, Brazil), at 30 °C. The samples were degassed (with N_2) to avoid the interference of dissolved O_2 in the longitudinal relaxation (T_1) and nuclear Overhauser (ROESY) measurements. For ^1H NMR, a 90° pulse was typically of 10–15 s, and the recycling time was set to 5 times the largest T_1 (those of the aromatic hydrogens of ATC) in the samples. Longitudinal relaxation times were obtained by the conventional inversion-recovery technique. 2D-NOE experiments used the ROESY sequence [23]; the spectral width was typically 8000 Hz and 648 τ_1 increments were recorded with 64 transients of 2 K complex points, for each free induction decay. The ROESY experiments were carried out using a mixing time of 150 ms and 300 ms for the detection of build-up NOEs [24,25]. The NMR spectra were referenced to the residual water peak, adjusted for 3.9 ppm [26,27].

Data were processed using the NMRPipe and NMRView software. Prior to Fourier transformation, the time domain data were zero-filled in both dimensions in order to yield an 8 K × 2 K data matrix. When necessary, a fifth-order polynomial baseline correction was applied after transformation and phasing. The intermolecular distances were determined using the 300 ms ROESY spectrum and the cross-peaks volumes were directly correlated with inter-nuclear distance (r) of the two observed hydrogens, via the known r^{-6} dependence [28]. The intramolecular distance between hydrogen "*h*" (see assignments in Table 1) and the methyl group (*g*) attached to the thiophene ring of articaine (3.06 Å) was used for calibration.

2.5. Molecular dynamics simulations

MD simulations were conducted for both neutral and protonated forms of ATC (nATC and pATC, respectively) species in lipid bilayers. The simulated systems consisted of a bilayer containing 126 POPC molecules (63 lipids in each monolayer), 4580 water molecules and a single ATC molecule (nATC or pATC). The complete simulated systems were assembled with Packmol [29]. The simulation box was periodically replicated. The simulations were conducted with the NAMD program [30], using the CHARMM36 lipid force field [31]. The CHARMM-based parametrization procedure of nATC has been described in a previous study [32]. The partial atomic charges of pATC were calculated using the same protocol described in that reference, and all other parameters were directly transferred from nATC. The water molecules were described with the TIP3P model [33].

Simulations were performed in the NP_zAT ensemble (constant

Table 1
Chemical shifts in the ^{1}H NMR spectra of nATC, EPC, and nATC:EPC samples[a].

Assignment[a]		Chemical Shift (δ, ppm)			Δδ (ppm)
Peak		nATC/D_2O	EPC	nATC:EPC	
A	ω-CH_3		0.000	0.003	+0.003
a	**N–C–C–CH_3**	**0.047**		**0.088**	+ **0.041**
B	$(CH_2)_n$		0.400	0.408	+0.008
b	CO-C-CH_3	**0.551**		**0.606**	+ **0.055**
c	**N–C–CH_2–C**	**0.661**		**0.701**[b]	-[c]
C	β-CH_2		0.691	0.699	+0.008
D	CH_2C=C		1.153	1.152	+0.001
d	**=C–CH_3**	**1.220**		**1.255**	+ **0.035**
E	α-CH_2		1.492	1.491	−0.001
e	**N–CH_2–C–C**	**1.742**		**1.893**[b]	-[c]
F	=C–CH_2–C=		1.916	1.923	+0.007
G	$N^+(CH_3)_3$		2.358	2.367	+0.009
f	**CO–CH–N**	**2.733**		-	-[c]
H	CH_2–N^+		2.801	2.809	+0.008
g	**-O-CH_3**	**2.982**		**2.960**	**−0.022**
I	O_3PO-CH_2 (choline)		3.338	3.355	+0.017
J	O_3PO-CH_2 (glycerol)		3.404	3.412	+0.008
K	CH_2–OCO		3.545	3.534	−0.011
L	CH–OCO[d]		4.421	4.429	+0.008
h	**H–C=**	**6.597**		**6.435**	**−0.162**

[a] Capital letters refer to EPC; lower-case letters refer to ATC peaks (assignments depicted in Fig. 2).
[b] Determined from the ROESY experiments.
[c] Peaks not detected because of spectral superposition.
[d] CH=CH hydrogens, from unsaturated acyl chain of EPC can be also superposed here.

number of atoms, normal pressure, superficial area and temperature), which is appropriate to be associated with the CHARMM force field in simulations of biomembranes. The size of the simulation cell was adjusted to accommodate the 63 lipids on each monolayer (L_x = 62.8 Å and L_y = 65.1 Å) to give an area per lipid corresponding to 64 Å^2. Temperature and pressure were kept constant at 310 K and 1 atm, respectively. Initially, the energy of the system was minimized by 500 conjugate gradient (CG) steps as implemented in NAMD [34]. This was followed by three 20 ns equilibration independent simulations were run over 20 ns One simulation of each system (nATC and pATC) was extended up to 100 ns We have skipped the first 12 ns of the extended trajectories and used the remaining 88 ns to compute different statistical properties of systems. A multiple-time step algorithm, RESPA [35], with the shortest time step of 2 fs was used. During the simulation, all intramolecular motions involving hydrogen atoms were frozen using the SHAKE algorithm [36]. The short-range forces were computed using a cutoff of 10 Å (with a smooth decay from 8 Å) and the long-range forces were taken into account by means of the particle mesh Ewald (PME) method [37].

We chose the adaptative biasing-force (ABF) method to compute the free energy profile that describes the energetics of one ATC molecule crossing a membrane bilayer and find the barriers and minima that determine its preferential position in the system. Briefly, the ABF method consists of performing simulations with no constraints and computing the free energy profile to one more reaction coordinates of interest, ξ, by generating an ensemble of average forces that act on the atoms along ξ. In practice, the values of external force towards the molecule are sampled during the simulation for small discrete intervals of ξ. Every time the system visits that piece of ξ a force with same the module of the computed average force but with opposite direction is applied to the atoms of interest, so that the sum of forces is, on average, null. As a result, the dynamics in the reaction coordinate progressively becomes closely diffusive, enabling enough sampling at less energetically favorable regions of ξ. A more complete and rigorous theoretical description of ABF method is found elsewhere [38].

Here, we chose as the reaction coordinate the distance between the center of mass of ATC and a reference point centrally placed in the simulation box, *i.e.*, in the middle of the water layer. Thus, the free energy profile was computed across the trajectory of the center of mass of ATC from the center of the water layer to the center of the bilayer. In order to avoid the translational motion of the membrane, we set harmonic constraints with force constants of 1000 kcal/mol/Å over ~30% of the phosphorous atoms of the lipid heads in the opposite layer relative to ATC penetration. The reaction coordinate was divided in windows of ~4 Å so that the simulations in these intervals could be conducted in parallel. The translation of the center of mass of articaine was restricted to each region by boundary potentials with a force of 10 kcal/mol. Forces along each window were estimated with a precision of 0.1 Å and the simulations were performed so that the forces at each point of the reaction coordinate were collected, at least, 1,000,000 times. Using the number of samples in each point and the correspondent average force from the windows simulations, we performed a final run, screening all the extension - from water to the center of the membrane - with no segmentations. Altogether, the simulations took *ca.* 0.8 μs.

3. Results and discussion

Local anesthetics have to diffuse trough biological membranes in order to promote anesthesia [3,39]. The same is true for model (lipid membranes) where LA have also a preferential site, where they are found for most of the time inside the bilayer [27,40–43]. The depth of such penetration is higher for the uncharged than for the charged species [44,45] and changes according to the partition coefficient of the anesthetic [42]. The following experiments were conducted to track the average preferential position of ATC in lipid bilayers.

3.1. Static fluorescence studies indicate the superficial insertion of nATC in lipid membranes

The intrinsic emission of nATC was measured at pH 9.0, and its anisotropy of fluorescence was calculated both in water (0.03) and

in the presence of 0.5 mM EPC vesicles (0.29). The random movement of the anesthetic in solution gave way to a preferential orientation in the bilayer. Anisotropy was a strong evidence of nATC partitioning into the lipid bilayers, where they got oriented and follow the slow tumbling regimen of the vesicles [46].

We have also employed AHBA, a probe designed to monitor the membrane surface milieu [21], to follow nATC interaction with EPC membranes, at pH 9.0. Fig. 1 shows a decline in the fluorescence intensity of the fluorophore with the increase in the nATC concentration. The quenching of AHBA's fluorescence indicated the presence of nATC molecules in the milieu of the probe, at the polar head group region of the bilayer, indicating a superficial insertion of neutral ATC in unilamellar EPC liposomes.

3.2. ^1H NMR experiments

NMR was applied to investigate the interaction between uncharged ATC and EPC bilayers and to detect any preferential location of the anesthetic inside the bilayer. Fig. 2 shows ^1H NMR spectra of nATC, control liposomes (EPC), and nATC + EPC samples

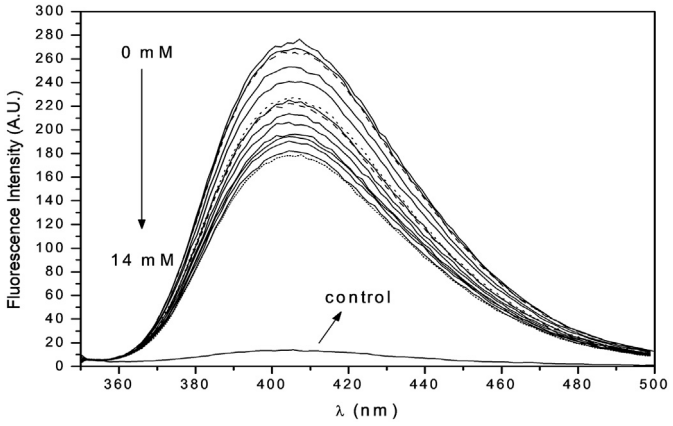

Fig. 1. Fluorescence quenching of AHBA (10^{-5} M) probe induced by nATC (0–14 mM). The probe was inserted into 0.5 mM EPC unilamellar liposomes. The control sample refers to liposomes in 0.025 M borate buffer, at pH 9.0.

and discloses the assignments of the hydrogen signals for [40,47] and ATC [16,21] which are in good agreement with previous reports. Table 1 compiles the results obtained in the spectra of Fig. 2. Thus, the assignment of hydrogen signals (capital and lowercase letters for EPC and ATC, respectively) is given as a function of the chemical Shift (δ, ppm) in the spectra of the compounds alone and in the nATC:EPC sample. From these results, it was possible to calculate the variation of the chemical shift ($\Delta\delta$), in relation to the pure compound for each hydrogen signal. It can be noticed that nearly all signals referring to EPC were slightly shifted to higher magnetic fields in the presence of nATC. This shift probably results from the ring current effect of the delocalized π-electron system of nATC, as previously reported for local anesthetics and flavonoids in lipid bilayers [42,43]. Although no huge changes in the chemical shift of EPC hydrogens ($|\Delta\delta| < 0.02$ ppm) were detected in the presence of nATC, the major deviation affected the vicinity of O_3PO-CH_2 choline hydrogens (peak I, $\Delta\delta = +0.017$), compatible with nATC being at the polar head group region [42,43].

Most importantly, Table 1 also reveals changes in the chemical shift of ATC hydrogens between D_2O and EPC vesicles. Major deviations ($|\Delta\delta| > 0.05$ ppm) were observed for peaks **h** (upfield) and **b** (downfield). Besides, articaine signals got broadened (Fig. 2) in the presence of EPC vesicles, indicating that the anesthetic molecule lost mobility by inserting in-between the lipids (as also evidenced by the fluorescence anisotropy results).

3.3. T_1 analysis

Measurements of ^1H NMR longitudinal relaxation times (T_1) provided information about the dynamics of hydrogens atoms in nATC, EPC, and nATC:EPC samples. Table 2 shows the T_1 values measured for nATC hydrogens in D_2O (isotropic environment) and in the presence of EPC vesicles (anisotropic environment). ΔT_1 values reveal a clear reduction on the dynamics of all articaine hydrogens in the presence of EPC vesicles, with the aromatic thiophene hydrogen (peak **h**) and the methyl hydrogens nearby the amine group (peak **a**) being the most affected. This result, in agreement with the observed broadening of the ^1H resonance peaks (Fig. 2) and fluorescence anisotropy data, indicates restriction in the mobility of the nATC molecules, as if it was fully inserted

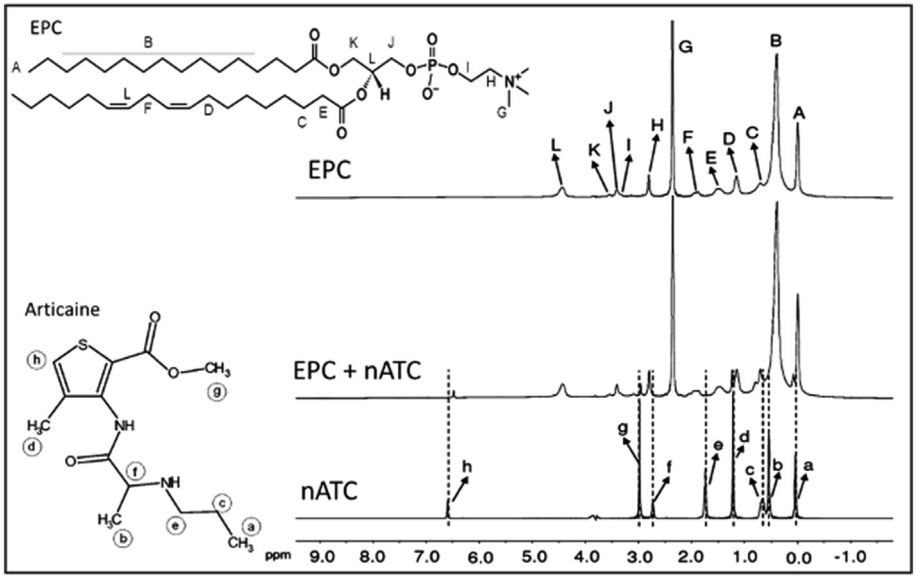

Fig. 2. 500 MHz ^1H NMR spectra of EPC small unilamellar vesicles, nATC + EPC, and nATC, at pH 9.4 and 30 °C. Peak assignments are given in Table 1.

Table 2
T_1 values of nATC hydrogens in the absence and presence of EPC vesicles. Experimental conditions are the same as described in Fig. 2.

Peaks	T_1 (s)		
	nATC	nATC:EPC	ΔT_1 (s)
a	1.855 ± 0.029	0.773 ± 0.057	1.082
b	0.735 ± 0.007	0.553 ± 0.031	0.182
c	1.246 ± 0.023	[a]	
d	1.112 ± 0.034	0.971 ± 0.004	0.141
e	0.817 ± 0.019	[a]	
f	1.781 ± 0.023	[a]	
g	1.429 ± 0.035	1.234 ± 0.036	0.195
h	5.627 ± 0.014	3.523 ± 0.023	2.104

[a] Not determined due to peak superposition.

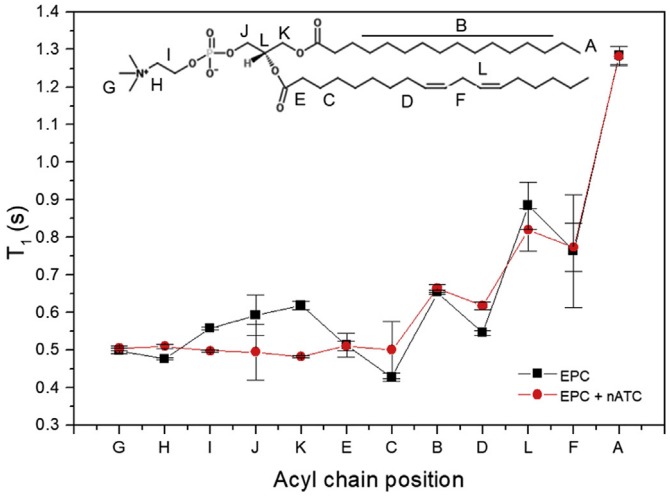

Fig. 3. Effect of nATC on the longitudinal relaxation times of EPC hydrogens, measured at 30 °C, pH 9.4, and 500 MHz. The hydrogen signals (assigned as in Table 1) are placed accordingly to their position in an EPC molecule depicted with the polar head-group (left) and acyl chain regions (right) [42,47].

into the lipid bilayer [42].

An analysis of the T_1 values of EPC measured in the presence of neutral articaine reveals specific regions of the lipid molecule that were mostly affected by the insertion of the anesthetic between lipids (Fig. 3). Major changes (decreased T_1 values) were noted for peaks K, J, and I, corresponding to glycerol and choline hydrogens, nearby the phosphate group of EPC. The glycerol moiety is known to be the most restricted region in the bilayer packing, so that any additional decrease in the mobility of those hydrogens can be only ascribed to the presence of the anesthetic in that spot [40,42].

Interestingly, similar decreases in T_1 values from hydrogens in the vicinity of PO_4^- and glycerol moiety (peaks I, J, K) have been previously observed for the insertion of other amino-amide local anesthetics (lidocaine and mepivacaine) into EPC vesicles [42], but not for their analogs of higher hydrophobicity (etidocaine and bupivacaine). In such way, nATC behavior resembles that of the less hydrophobic LA, lidocaine, mepivacaine [42] and prilocaine [45,48], rather than more lipophilic local anesthetic agents.

3.4. ROESY experiments

Nuclear Overhauser (ROESY) experiments (Fig. 4) were run in an attempt to determine putative intermolecular (nATC − EPC) interactions that would help to confirm the preferential location of articaine molecules inside the lipid bilayer.

Four intermolecular cross-peaks were determined in the ROESY

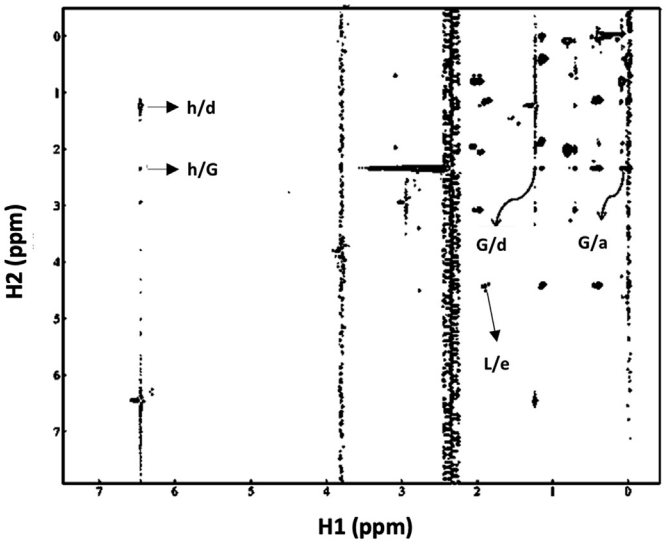

Fig. 4. ROESY spectrum of nATC (130 mM) in EPC (100 mM) liposomes at pH 9.4, revealing one intramolecular cross-peak (between hydrogens *d* and *h* of articaine), and four intermolecular cross-peaks (between EPC and articaine, capital/lower letters − see assignments in Table 1). 500 MHz, 300 ms mixing time, 37 °C.

spectrum of nATC-EPC, between hydrogens belonging to articaine (peaks **a**, **d**, **e**, and **h**) and to the lipid (peaks G and L) molecules. These spatial proximities confirm the superficial insertion of nATC in the lipid bilayer, once the main interactions of articaine involved choline (peak G) and glycerol (peak L) hydrogens of the EPC molecule. The volume of each cross-peak was measured, and intermolecular distances were calculated, as described in Methods. The calculated distances between G-**d**; G-**a**; L-**e**; and G-**h** were 4.8 Å, 5.2 Å, 5.8 Å, and 6.0 Å, respectively.

At this point, the spectroscopic tools used to examine the nATC in liposomes system had provided important information on the dynamics and topology of the interaction. Next, further characterization was conducted through computational simulations of the interaction of articaine with model bilayers. POPC was the lipid chosen to perform the molecular dynamic simulations, since palmitic (C16:0) and oleic (C18:1) are the most abundant fatty acids in *sn-1* and *sn-2* chains of phosphatidylcholine from egg yolk [49] and plasma membranes [50].

3.5. Computational studies

In a first approach, independent MD simulations were conducted starting with a single nATC in the water phase, applying the NP_zAT ensemble. Fig. 5 shows the trajectory of the center of mass of a nATC molecule projected onto an axis normal to the bilayer surface (z_m direction). The average position of phosphate P atoms in the lipid heads of a monolayer was taken as reference ($z_m = 0$, black circles in Fig. 5). In this Figure, one can see the diffusion of the nATCs into the interior of the bilayer. It took between 3 and 11 ns for the diffusion to happen in this (64 $Å^2$ area per lipid molecule) bilayer [19]. Similar results were obtained for areas of 68 $Å^2$ and 73 $Å^2$ (data not shown).

For comparison, the simulation of pATC in the same conditions gave different results, with no insertion of the pATC into the lipid bilayer (data not shown). Because of this, we have simulated one case in which one pATC was originally placed inside the lipid bilayer. The trajectory of the center of mass of pATC (Fig. 5) shows that it remained in the water-lipid interface during the simulation.

We did not observe any articaine crossing events between POPC

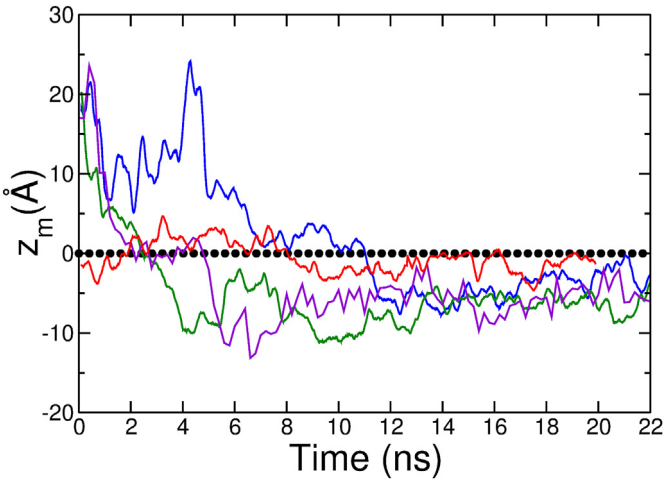

Fig. 5. Articaine center of mass trajectories relative to the average position of the upper leaflet phosphorous atoms. The green, blue, and violet curves correspond to nATC in three independent simulations. In red, for comparison purpose, we show a selected trajectory of a pATC molecule, initially placed directly inside the bilayer (see text).

monolayers during 100 ns of simulation. It is important to notice that we considered a single ATC in our simulations (infinite dilution). Other authors reported [11,18] articaine crossing events between DMPC monolayers at high ATC concentrations, as seen for other anesthetic molecules [45], also at high concentrations. This difference could suggest that ATC cooperative effects (at high concentration) may favor them. However, more extensive sampling at infinite dilution is needed to fully verify this hypothesis.

The arrangement of the system was evaluated by means of the electron density profile (EDP) across the simulation box. The profiles were calculated by time- averaging the electron density per 0.1 Å thick windows in the z-axis, assuming that each atom concentrates a number of electrons equal to the atomic number of the corresponding chemical element. Fig. 6A shows the EDP of nATC and pATC. The EDP profiles of POPC and water from the nATC system are also represented for reference. The center of the bilayer corresponds to z = 0. The nATC molecule is essentially located below the lipid head/lipid tails interfacial region, at ~14 Å from the bilayer center – *i.e.*, at the glycerol region – typically where more hydrophilic anesthetics are found [48]. In contrast, pATC curve shows that the charged form is mostly found slightly closer to the water, essentially at the polar head/water interface (at ~15 Å from the bilayer center). The distance between nATC and pATC distribution peaks (~1 Å) is in agreement with a previous work, in which an NPT ensemble was used [48].

Here, we used the adaptative-biasing force method to describe the free energy surface underlying the favorable penetration of nATC into the POPC membrane. In agreement with the computed electron density profile, the resulting potential mean force across the bilayer (Fig. 6B) shows a large valley (~13 Å wide), with the lowest ΔG value at ~12 Å from the center of the bilayer, and a slight increase at the lipid head region (~15 Å).

In order to describe in detail, the conformation and orientation of the articaine molecules inside the bilayer, we plotted separately the EDP of the four methyl groups present in the LA molecule (Fig. 7). There is a clear difference in insertion of the methyl groups *a* and *g* (facing the interior of the bilayer) *vs.* CH_3 groups *b* and *d* (oriented towards the water/lipid interface) of nATC. As described elsewhere [16], the ATC tail (containing the *a* and *b* methyl groups) shows more restricted mobility in POPC bilayers than in the water phase (where the tail freely rotates). This observation is in very good agreement with the decrease in T_1 values of nATC observed in the presence of liposomes (Table 2). In contrast, in the case of pATC the differences among the 4 methyl groups are not so clear; and the EDP of the *b* group shifted *ca.* 6 Å from the bilayer center in comparison to nATC, as a result of its proximity to the protonated nitrogen atom (now facing the water phase) of articaine.

Skjevik and co-workers, in a molecular dynamics study, describe the formation of an intramolecular hydrogen bond (HB) in nATC

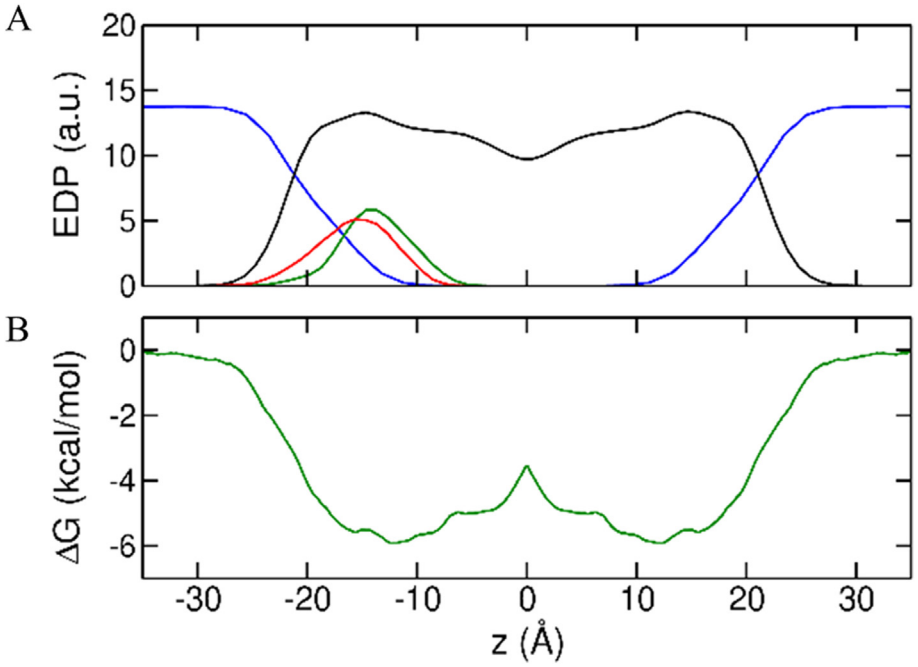

Fig. 6. A) Electron density profiles (a.u. = arbitrary units) of nATC (green), pATC (red), water (blue), and POPC (black). The ATC densities were amplified 24 times for visualization purposes. **B**) Gibbs free energy profile of nATC in a POPC lipid bilayer.

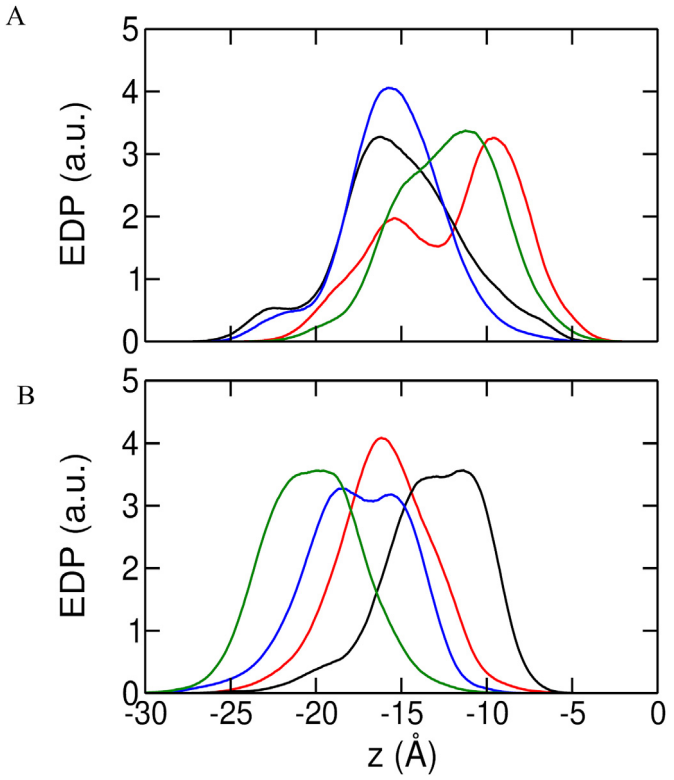

Fig. 7. Electron density profiles of the methyl groups of nATC (**A**) and pATC (**B**) in the partitioning into POPC bilayers. The represented EDP distribution corresponds to the methyl groups: *a* (green), *b* (blue), *d* (black), and *g* (red) of the articaine molecule.

when inserted into a POPC membrane [19]. According to these authors, in the bilayer, this hydrogen bond decreases the exposure of nATC to hydrophilic sites, making it more stable in hydrophobic environments. In fact, our results show that the nATC molecule, when inserted in POPC, resembles the *horseshoe* shape of the optimized structure in gas phase. However, this does not suggest higher lipophilicity of articaine in comparison to other LA, since its insertion in the bilayer is superficial, as supported by the NMR experiments.

We observed that nATC formed hydrogen bonds with POPC during only ~4% of the simulation time, while it interacts by one HB with water during ~46% of the simulation time. A more detailed analysis shows that the main groups that interact are the amine hydrogen of the nATC with the ester carbonyl oxygen of the POPC acyl chain, and the amide oxygen in articaine with the water hydrogen, as shown in the snapshot of Fig. 8 and represented in Fig. S1.

The pATC molecules interacted during most of the simulation time by HBs with the water molecules and one HB with the POPC lipids (61 and 81% of the simulation time, respectively). During most of the simulation time, the hydrogen atoms from amide and amine group of pATC interact simultaneously with a phosphate carbonyl oxygen of POPC. The protonated amine group of articaine is the main contributor for the high frequency of the hydrogen bonds established with water. We did not observe any intramolecular hydrogen bond occurring in the pATC.

Since the ROESY (NMR) spectrum revealed four intermolecular cross-peaks between hydrogens belonging to the ATC molecule and the lipid, in order to compare experimental and computational (MD) results we have calculated the radial distribution function, g(r), between selected hydrogens of POPC and nATC (Fig. S2). A first well- defined peak was observed at 5.3 Å for de g(r) between *L* hydrogen of POPC and *e* of nATC (see Table 1 for assignments). This shows a very good agreement with the ROESY results that revealed a 5.8 Å for this distance. For the other radial distribution functions, we did not find any well-defined structure.

In summary, by combining spectroscopic and simulation techniques we were able to demonstrate that the uncharged form of ATC interacts with PC bilayers in a specific orientation. nATC intrinsic fluorescence suggested a random orientation in water and a preferential orientation inside EPC vesicles, at pH 9.0. Besides, nATC was able to quench the fluorescence of AHBA probe in a concentration-dependent manner, suggesting a superficial insertion of the uncharged ATC into extruded EPC liposomes. The ^{1}H NMR signals of nATC were broadened in the presence of EPC

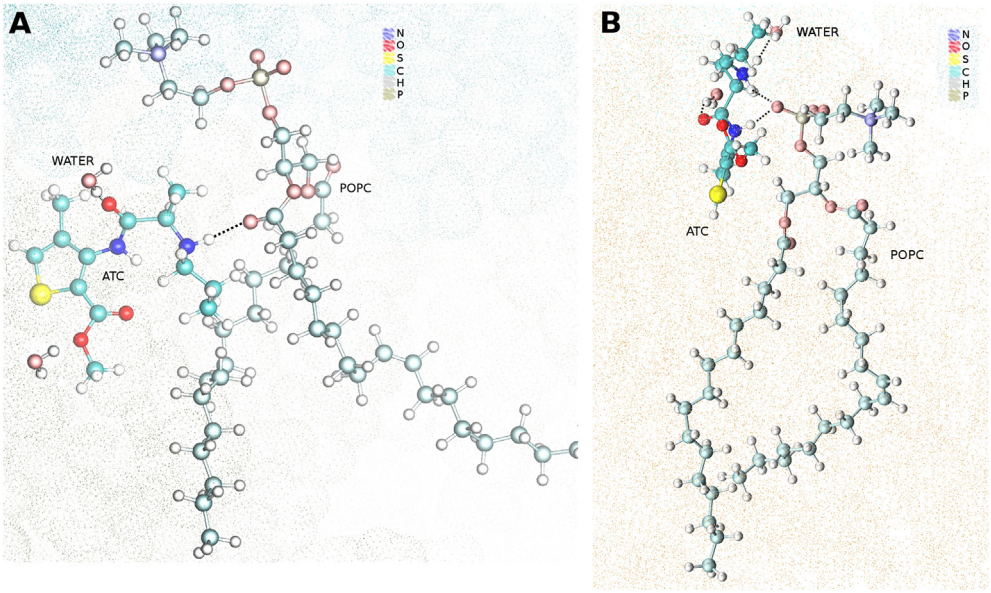

Fig. 8. Representative snapshots of MD simulations showing the conformation and relative position of the nATC molecule and a selected POPC lipid from two perspectives (A and B). The most frequent hydrogen bond types of nATC with POPC and with a water molecule are depicted (dashed lines).

vesicles relatively to signals in water, confirming the insertion of the anesthetic molecule into the EPC bilayer. Chemical shift changes were not significant for EPC hydrogens, but for hydrogens *b* and *h* of ATC. Analyses of the T_1 values revealed specific regions of the lipid molecule that were mostly affected by the insertion of ATC. Major changes (decreased T_1 values) were noted for peaks belonging to glycerol and choline hydrogens, nearby the phosphate group of EPC. Likely, ROESY experiments indicated that the preferential location of ATC molecule inside EPC bilayers was nearby the polar head group of the lipids. Molecular dynamics simulations showed that neutral ATC adopted a *horseshoe* shape in POPC lipid bilayers, being preferentially located at the glycerol region, in very good agreement with the experimental results.

4. Conclusion

The results of the experimental and computational approaches show that the insertion of articaine molecule in model membranes is quite similar to that of other hydrophilic LA (*e.g.* lidocaine, prilocaine, and mepivacaine), near the polar head group of the lipids. Moreover, our simulation results confirm that neutral articaine, differently than other anesthetic agents, adopts a *horseshoe* shape when inserted in phosphatidylcholine membranes.

Computational analyzes were deepened (relative to previous reports) to describe the preferential conformation of articaine in phospholipid membranes. In particular, we looked at the organization of the methyl groups of articaine, which allowed correlation with experimental (NMR) results, and detected formation of hydrogen bonds between articaine and the lipid heads.

In summary, the preferential location of articaine in the bilayer does not support the hydrophobic character usually assigned to it. Thus, the therapeutic improvement achieved with articaine should not be attributed to the putative lipophilicity, but possibly to its higher clinical doses, in comparison to lidocaine, prilocaine, and mepivacaine.

CRediT authorship contribution statement

Érica Teixeira Prates: Methodology, Investigation, Writing - review & editing. **Gustavo Henrique Rodrigues da Silva:** Methodology, Writing - original draft. **Thais F. Souza:** Methodology. **Munir S. Skaf:** Project administration, Investigation. **Mónica Pickholz:** Software, Conceptualization, Writing - review & editing. **Eneida de Paula:** Conceptualization, Funding acquisition, Writing - review & editing.

Declaration of competing interest

The authors declare they have no conflict of interest.

Acknowledgments

The authors are grateful to Dr. Leonardo F. Fraceto (São Paulo State University, UNESP/Sorocaba, SP, Brazil) for the collection and treatment of NMR data and Dr. Amando S. Ito (FFCLRP/USP) for providing the AHBA fluorophore. We also thank FAPESP (#07/02629-2; #14/14457-5 grant; #17/15174-5), CNPq (# 309625/2017-3), CONICET (# 0131-2014), ANPCyT (# PICT-2014-3653) for financial support and Aventis Pharma for kindly donate articaine.

Appendix A. Supplementary data

Supplementary data to this article can be found online at https://doi.org/10.1016/j.molstruc.2020.128854.

References

[1] G.R. Strichartz, Local Anesthetics, Springer Berlin Heidelberg, Berlin, Heidelberg, 1987, https://doi.org/10.1007/978-3-642-71110-7.
[2] E. de Paula, C.M.S. Cereda, L.F. Fraceto, D.R. de Araújo, M. Franz-Montan, G.R. Tofoli, J. Ranali, M.C. Volpato, F.C. Groppo, Micro and nanosystems for delivering local anesthetics, Expet Opin. Drug Deliv. 9 (2012) 1505–1524, https://doi.org/10.1517/17425247.2012.738664.
[3] D.R. de Araújo, L.N. de M. Ribeiro, E. de Paula, Lipid-based carriers for the delivery of local anesthetics, Expet Opin. Drug Deliv. 16 (2019) 701–714, https://doi.org/10.1080/17425247.2019.1629415.
[4] G.H. Rodrigues da Silva, L.N.M. Ribeiro, H. Mitsutake, V.A. Guilherme, S.R. Castro, R.J. Poppi, M.C. Breitkreitz, E. de Paula, N.L.C. Optimised, A nanotechnological approach to improve the anaesthetic effect of bupivacaine, Int. J. Pharm. 529 (2017) 253–263, https://doi.org/10.1016/j.ijpharm.2017.06.066.
[5] J.F. Butterworth IV, G.R. Strichartz, Molecular mechanisms of local anesthesia: a review, Anesthesiology 72 (1990) 711–734, https://doi.org/10.1097/00000542-199004000-00022.
[6] D.B. Tikhonov, B.S. Zhorov, Mechanism of sodium channel block by local anesthetics, antiarrhythmics, and anticonvulsants, J. Gen. Physiol. 149 (2017) 465–481, https://doi.org/10.1085/jgp.201611668.
[7] E. de Paula, S. Schreier, Molecular and physicochemical aspects of local anesthetic-membrane interaction, Braz. J. Med. Biol. Res. 29 (1996) 877–894.
[8] G.R. Seward, Handbook of Local Anesthesia, Elsevier, 1981, https://doi.org/10.1016/0300-5712(81)90017-8.
[9] A.J.G. Hopman, J.A. Baart, H.S. Brand, Articaine and neurotoxicity-A review, Br. Dent. J. 223 (2017) 501–506, https://doi.org/10.1038/sj.bdj.2017.782.
[10] S.F. Malamed, S. Gagnon, D. Leblanc, Efficacy of articaine: a new amide local anesthetic, J. Am. Dent. Assoc. 131 (2000) 635–642, https://doi.org/10.14219/jada.archive.2000.0237.
[11] M. Saeedi, A.P. Lyubartsev, S. Jalili, Anesthetics mechanism on a DMPC lipid membrane model: insights from molecular dynamics simulations, Biophys. Chem. 226 (2017) 1–13, https://doi.org/10.1016/j.bpc.2017.03.006.
[12] B.G. Covino, Pharmacology of local anaesthetic agents, Br. J. Anaesth. 58 (1986) 701–716.
[13] G. Lagan, H.A. McLure, Review of local anaesthetic agents, Curr. Anaesth. Crit. Care 15 (2004) 247–254, https://doi.org/10.1016/j.cacc.2004.08.007.
[14] A.L. Frankhuijzen, Pharmacology of local anaesthetics, Local Anaesth. Dent. (2017) 37, https://doi.org/10.1007/978-3-319-43705-7_3.
[15] S.F. Malamed, Handbook of Local Anesthesia, Elsevier, 2013.
[16] C. Song, H. Lygre, W. Nerdal, Articaine interaction with DSPC bilayer: a13C and31P solid-state NMR study, Eur. J. Pharmaceut. Sci. 33 (2008) 399–408, https://doi.org/10.1016/j.ejps.2008.01.010.
[17] H. Lygre, G. Moe, W. Nerdal, H. Holmsen, Interaction of articaine hydrochloride with prokaryotic membrane lipids, Acta Odontol. Scand. 67 (2009) 1–7, https://doi.org/10.1080/00016350802443466.
[18] E.H. Mojumdar, A.P. Lyubartsev, Molecular dynamics simulations of local anesthetic articaine in a lipid bilayer, Biophys. Chem. 153 (2010) 27–35, https://doi.org/10.1016/j.bpc.2010.10.001.
[19] Å.A. Skjevik, B.E. Haug, H. Lygre, K. Teigen, Intramolecular hydrogen bonding in articaine can be related to superior bone tissue penetration: a molecular dynamics study, Biophys. Chem. 154 (2011) 18–25, https://doi.org/10.1016/j.bpc.2010.12.002.
[20] M. Snoeck, Articaine: a review of its use for local and regional anesthesia, Local Reg. Anesth. 5 (2012) 23–33, https://doi.org/10.2147/LRA.S16682.
[21] C.A. Marquezin, I.Y. Hirata, L. Juliano, A.S. Ito, Spectroscopic characterization of 2-amino-N-hexadecyl-benzamide (AHBA), a new fluorescence probe for membranes, Biophys. Chem. 124 (2006) 125–133, https://doi.org/10.1016/j.bpc.2006.06.002.
[22] J.R. Lakowicz, Principles of Fluorescence Spectroscopy Principles of Fluorescence Spectroscopy, Springer, 2006, https://doi.org/10.1007/978-0-387-46312-4.
[23] A. Bax, D.G. Davis, Practical aspects of two-dimensional transverse NOE spectroscopy, J. Magn. Reson. 63 (1985) 207–213, https://doi.org/10.1016/0022-2364(85)90171-4.
[24] Y. Kuroda, K. Kitamura, Intra-and intermolecular 1H-1H nuclear overhauser effect studies on the interactions of chlorpromazine with lecithin vesicles, J. Am. Chem. Soc. 106 (1984) 1–6, https://doi.org/10.1021/ja00313a001.
[25] J. Baber, J.F. Ellena, D.S. Cafiso, Distribution of general anesthetics in phospholipid bilayers determined using 2H NMR and — NOE Spectroscopy1, Biochemistry 34 (1995) 6533–6539. https://pubs.acs.org/doi/pdf/10.1021/bi00019a035. (Accessed 26 May 2018).
[26] L.M.A. Pinto, D. Kiyoko Yokaichiya, L.F. Fraceto, E. de Paula, Interaction of benzocaine with model membranes, Biophys. Chem. 87 (2000) 213–223, https://doi.org/10.1016/S0301-4622(00)00196-4.
[27] L.F. Fraceto, L.M.A. Pinto, L. Franzoni, A.A.C. Braga, A. Spisni, S. Schreier, E. de Paula, Spectroscopic evidence for a preferential location of lidocaine inside phospholipid bilayers, Biophys. Chem. 99 (2002) 229–243, https://doi.org/10.1016/S0301-4622(02)00202-8.
[28] K. Wüthrich, NMR with proteins and nucleic acids, EuroPhys. News 17 (1986) 11–13, https://doi.org/10.1051/epn/19861701011.
[29] L. Martínez, R. Andrade, E.G. Birgin, J.M. Martínez, PACKMOL: a package for building initial configurations for molecular dynamics simulations, J. Comput.

Chem. 30 (2009) 2157–2164, https://doi.org/10.1002/jcc.21224.
[30] J.C. Phillips, R. Braun, W. Wang, J. Gumbart, E. Tajkhorshid, E. Villa, C. Chipot, R.D. Skeel, L. Kalé, K. Schulten, Scalable molecular dynamics with NAMD, J. Comput. Chem. 26 (2005) 1781–1802, https://doi.org/10.1002/jcc.20289.
[31] R.W. Pastor, A.D. MacKerell, Development of the CHARMM force field for lipids, J. Phys. Chem. Lett. 2 (2011) 1526–1532, https://doi.org/10.1021/jz200167q.
[32] E.T. Prates, P.C.T. Souza, M. Pickholz, M.S. Skaf, CHARMM-based parameterization of neutral articaine-a widely used local anesthetic, Int. J. Quant. Chem. 111 (2011) 1339–1345, https://doi.org/10.1002/qua.22701.
[33] W.L. Jorgensen, J. Chandrasekhar, J.D. Madura, R.W. Impey, M.L. Klein, Comparison of simple potential functions for simulating liquid water, J. Chem. Phys. 79 (1983) 926–935, https://doi.org/10.1063/1.445869.
[34] T. Darden, D. York, L. Pedersen, Particle mesh Ewald: an N·log(N) method for Ewald sums in large systems, J. Chem. Phys. 98 (1993) 10089–10092, https://doi.org/10.1063/1.464397.
[35] L. Kalé, R. Skeel, M. Bhandarkar, R. Brunner, A. Gursoy, N. Krawetz, J. Phillips, A. Shinozaki, K. Varadarajan, K. Schulten, NAMD2: greater scalability for parallel molecular dynamics, J. Comput. Phys. 151 (1999) 283–312, https://doi.org/10.1006/JCPH.1999.6201.
[36] M. Tuckerman, B.J. Berne, G.J. Martyna, Reversible multiple time scale molecular dynamics, J. Chem. Phys. 97 (1992) 1990–2001, https://doi.org/10.1063/1.463137.
[37] H.C. Andersen, Molecular dynamics simulations at constant pressure and/or temperature, J. Chem. Phys. 72 (1980) 2384–2393, https://doi.org/10.1063/1.439486.
[38] E. Darve, D. Rodríguez-Gómez, A. Pohorille, Adaptive biasing force method for scalar and vector free energy calculations, J. Chem. Phys. 128 (2008) 144120, https://doi.org/10.1063/1.2829861.
[39] H. Tsuchiya, M. Mizogami, Interaction of local anesthetics with biomembranes consisting of phospholipids and cholesterol: mechanistic and clinical implications for anesthetic and cardiotoxic effects, Anesthesiol. Res. Pract. (2013), https://doi.org/10.1155/2013/297141.
[40] E. de Paula, S. Schreier, H.C. Jarrell, L.F. Fraceto, Preferential location of lidocaine and etidocaine in lecithin bilayers as determined by EPR, fluorescence and 2H NMR, Biophys. Chem. 132 (2008) 47–54. https://www.sciencedirect.com/science/article/pii/S0301462207002384. (Accessed 26 May 2018).
[41] N. Weizenmann, D. Huster, H.A. Scheidt, Interaction of local anesthetics with lipid bilayers investigated by 1H MAS NMR spectroscopy, Biochim. Biophys. Acta Biomembr. 1818 (2012) 3010–3018, https://doi.org/10.1016/j.bbamem.2012.07.014.
[42] L.F. Fraceto, A. Spisni, S. Schreier, E. de Paula, Differential effects of uncharged aminoamide local anesthetics on phospholipid bilayers, as monitored by 1H-NMR measurements, Biophys. Chem. 115 (2005) 11–18, https://doi.org/10.1016/j.bpc.2004.12.003.
[43] H.A. Scheidt, A. Pampel, L. Nissler, R. Gebhardt, D. Huster, Investigation of the membrane localization and distribution of flavonoids by high-resolution magic angle spinning NMR spectroscopy, Biochim. Biophys. Acta Biomembr. 1663 (2004) 97–107, https://doi.org/10.1016/j.bbamem.2004.02.004.
[44] M. Pickholz, L.F. Fraceto, E. de Paula, Distribution of neutral prilocaine in a phospholipid bilayer: insights from molecular dynamics simulations, J. Quant. Chem. 108 (2008) 2386–2391, https://doi.org/10.1002/qua.21767.
[45] L.F. Cabeca, M. Pickholz, E. de Paula, A.J. Marsaioli, Liposome–Prilocaine interaction mapping evaluated through STD NMR and molecular dynamics simulations, J. Phys. Chem. B 113 (2009) 2365–2370, https://doi.org/10.1021/jp8069496.
[46] K. Kinosita, S. Kawato, A. Ikegami, A theory of fluorescence polarization decay in membranes, Biophys. J. 20 (1977) 289–305, https://doi.org/10.1016/S0006-3495(77)85550-1.
[47] T. Darden, D. York, L. Pedersen, Particle mesh Ewald: an N·log(N) method for Ewald sums in large systems, J. Chem. Phys. 98 (1993) 10089–10092, https://doi.org/10.1063/1.464397.
[48] M. Pickholz, L.F. Fraceto, E. de Paula, Preferential location of prilocaine and etidocaine in phospholipid bilayers: a molecular dynamics study, Synth. Met. 159 (2009) 2157–2158, https://doi.org/10.1016/J.SYNTHMET.2009.07.034.
[49] S. Grobas, J. Mendez, R. Lazaro, C. de Blas, G.G. Mateo, Influence of source and percentage of fat added to diet on performance and fatty acid composition of egg yolks of two strains of laying hens, Poultry Sci. 80 (2001) 1171–1179, https://doi.org/10.1093/ps/80.8.1171.
[50] K. Leidl, G. Liebisch, D. Richter, G. Schmitz, Mass spectrometric analysis of lipid species of human circulating blood cells, Biochim. Biophys. Acta Mol. Cell Biol. Lipids 1781 (2008) 655–664, https://doi.org/10.1016/J.BBALIP.2008.07.008.